

Journal of Materials Chemistry A

Accepted Manuscript



This is an *Accepted Manuscript*, which has been through the Royal Society of Chemistry peer review process and has been accepted for publication.

Accepted Manuscripts are published online shortly after acceptance, before technical editing, formatting and proof reading. Using this free service, authors can make their results available to the community, in citable form, before we publish the edited article. We will replace this *Accepted Manuscript* with the edited and formatted *Advance Article* as soon as it is available.

You can find more information about *Accepted Manuscripts* in the [Information for Authors](#).

Please note that technical editing may introduce minor changes to the text and/or graphics, which may alter content. The journal's standard [Terms & Conditions](#) and the [Ethical guidelines](#) still apply. In no event shall the Royal Society of Chemistry be held responsible for any errors or omissions in this *Accepted Manuscript* or any consequences arising from the use of any information it contains.



Journal Name

ARTICLE

A conductive polymer coated MoO₃ anode enables an Al-ion capacitor with high performance

Received 00th January 20xx,
Accepted 00th January 20xx

DOI: 10.1039/x0xx00000x

www.rsc.org/

Faxing Wang,^{a,c,#} Zaichun Liu,^{b,#} Xiaowei Wang,^c Xinhai Yuan,^b Xiongwei Wu,^{b,*} Yusong Zhu^a, Lijun Fu^{a,*} and Yuping Wu^{*a,b,c}

Electrochemical capacitors are becoming the promising energy conversion/storage and power output devices. However, the high cost and low energy density are two serious disadvantages. By integrating the advantages of Li-/Na-ion batteries and electrochemical capacitors, the Li-/Na-ion capacitors are explored recently. Al is very cheap and the most abundant metal element on the earth. There is few report on Al-ion capacitor due to the challenges to find suitable anode with large capacitance and good rate performance. Here, the feasibility of assembling an Al-ion capacitor with good electrochemical performance is demonstrated. The Al-ion capacitor is enabled by using a composite of MoO₃ nanotubes coated by a conductive polypyrrole (PPy@MoO₃) as an anode, which functions via a redox intercalation/deintercalation of Al³⁺ ions in aqueous solution. It delivers a capacitance of 693 F g⁻¹, about 3 times higher than that of electrode materials for sodium-ion capacitor in aqueous solution. Combined with activated carbon (AC) cathode, the Al-ion capacitor presents an energy density of 30 Wh kg⁻¹ and an excellent cycling life with 93% capacitance retention after 1800 cycles. This finding provides another energy storage device with low cost and promote the application of capacitors.

Introduction

Considering the ever-growing demand for portable electronic devices and electric vehicles (EVs), supercapacitors and rechargeable batteries are emerging as two important classes of energy storage devices.^{1,2} The first supercapacitor patent was filed by General Electric as early as 1957, and since 1990 supercapacitors have drawn more and more attention in the field of hybrid electric vehicles due to their high power densities. In the case of lithium ion batteries, they were commercialized in the early 1990s as one of the most important and advanced rechargeable batteries because of their very high energy densities. A decade later, a new concept, Li-ion capacitor, was proposed for another breakthrough, which integrated the advantages of both Li-ion batteries (high energy density) and supercapacitors (high power density).^{3,4} Li-ion capacitors are usually assembled by a capacitor-type electrode and a Li-ion battery-type electrode with a Li-salt-containing electrolyte. Compared to conventional

carbon/carbon supercapacitors and asymmetric supercapacitors, the Li-ion capacitors deliver markedly increased energy density and high working voltage.³⁻⁸ However, the use of flammable organic electrolytes might lead to thermal run-away and safety accidents.⁹ So a lot of aqueous alkali-ion capacitors were also suggested such as AC//M_xMnO₂ (M= Li, Na and K) and AC//MnO₂ in aqueous electrolytes containing alkali metal ions.¹⁰⁻¹² Similar to the petroleum, the huge exploitation on Li resources driven by ever-growing demands in EVs and large grids will eventually lead to the depletion of Li resources since the lithium reserves are limited. Consequently, pursuing sustainable energy storage devices become increasingly important. Compared to Li resources, aluminum (Al) elements are abundant over the world with much lower price.

Recently, rechargeable Al-ion batteries in ionic liquid and aqueous electrolytes came into birth.¹³⁻¹⁶ Al-based energy storage devices show dominant advantages over the Li- or Na-ion capacitors: (1) Aluminum is the most abundant metal element in the Earth's crust; and (2) aluminum-based redox couple engages a three-electron transportation during the electrochemical charge/discharge reactions, which offers viable storage capacity relative to the Li- or Na-ion capacitors from single electron. However, there is few touch on Al-ion capacitor. The main reason is that there are rare electrode materials for Al-ion capacitors with good electrochemical performance. For example, the recently reported Ti₃C₂ only delivers a capacitance of less than 30 F g⁻¹ under the potential range of -0.65 – 0 V (vs. Ag/AgCl) in aqueous Al₂(SO₄)₃ electrolyte.¹⁷

^a College of Energy and Institute for Electrochemical Energy Storage, Nanjing Tech University, Nanjing 211816, Jiangsu Province, China. lijunfufu@sina.cn,

^b College of Science, Hunan Agriculture University, Changsha, Hunan 410128, China, wangnawxw@163.com.

^c New Energy and Materials Laboratory (NEML), Department of Chemistry, Fudan University, Shanghai 200433, China. E-mail: wuyyp@fudan.edu.cn.

#: Equal contribution to this work.

Electronic Supplementary Information (ESI) available: Thermogravimetric analysis of the MoO₃ nanotubes, TEM micrograph of the MoO₃ nanotubes, SAED pattern for PPy layer, CV curves of AC and MoO₃ nanotubes, change of capacitance with current densities for MoO₃ nanotubes, typical charge/discharge curves of AC and PPy@MoO₃ electrodes, change of capacitance with current densities and Coulombic efficiency for the Al-ion capacitor. See DOI: 10.1039/x0xx00000x

At the same time, nanostructured MoO₃ with various morphologies have been extensively investigated as the electrode materials for energy storage devices, for example, porous architectures,^{18a, 18b} nanowires,^{18c} nanobelt,^{18d,18e,18f} and nanoplate.¹⁹ More importantly, nanostructured MoO₃ with various morphologies significantly enhances the reversible ion insertion–extraction kinetics for supercapacitors and various batteries (Li ion battery, Na ionbattery, and Mg ion battery). However, no studies are available on the intercalation of Al³⁺ ions between the MoO₃ layers to the best of our knowledge. In this paper, we report an Al-ion capacitor with high energy density, excellent cycling life and good rate capability, which is realized by using PPy coated MoO₃ nanotubes as the anode and AC as the cathode in Al₂(SO₄)₃ aqueous solution. The redox intercalation/deintercalation of Al³⁺ ions into/out MoO₃ in aqueous solution was investigated by cyclic voltammograms(CV), ex-situ X-ray diffraction (XRD), X-ray photoelectron spectroscopy (XPS), elemental mappings and first-principles calculations. This work presents another step toward a world of “beyond lithium-ion” in sustainable energy storage devices.

Experimental

Synthesis of the materials

First, the carbon fibers purchased from Showa Denko were dispersed in concentrated nitric acid to remove some impurities and to endow the surface with hydrophilic groups. These carbon fibers were then filtered to form a film. An aqueous solution composed of 0.2 mol l⁻¹ molybdenum peroxy electrolyte was used to coat MoO_{3-x} on the as-formed carbon fiber film at a constant voltage of -0.6 V versus saturated calomel electrode (SCE). Molybdenum peroxy electrolyte was prepared by dissolving a proper amount of molybdenum powder (Aldrich) in 10 mL of 30% hydrogen peroxide. Then the MoO_{3-x}-coated carbon fibers were heat-treated at 500 °C for 5 hours to remove the carbon fibers. After the calcination process, the targeted MoO₃ nanotubes were achieved.

The PPy@MoO₃ nanotubes were prepared through the chemical polymerization of pyrrole (Py) on the MoO₃ nanotubes. Briefly, MoO₃ nanotube (0.2 g) were dispersed into a 150 ml solution containing 1 mg ml⁻¹ of sodium dodecylbenzenesulfonate (NaDBS). Upon stirring this mixture at 0 °C under the ice bath, 0.10 ml of Py monomer and 10 ml of 0.1 mol l⁻¹ FeCl₃ solution were added sequentially. The resulting precipitate was filtered and washed with water and acetone, and finally dried at 50 °C for 12 h under vacuum.

Material characterization

X-ray diffraction (XRD) patterns were collected using a BrukerD4 X-ray diffractometer (Bruker, Germany) with Ni-filtered CuK_α radiation (40 kV, 40 mA). Scanning electron micrographs (SEM) were obtained with a Philip XL30 microscope (Philips, The Netherlands) operated at 25 kV. Transmission electron micrographs (TEM) were acquired using a JEOL JEM-2010 transmission electron microscope (JEOL, Japan) operated at 200 kV. Samples were first dispersed in

ethanol and then collected using carbon-film-covered copper grids for analysis. Thermogravimetric analysis were carried out by utilizing a Perkin-Elmer TGA7/DSC7. Surface electronic states were investigated by X-ray photoelectron spectroscopy (XPS; Perkin-Elmer PHI 5000C ESCA, using Al KR radiation) and the binding energy values were calibrated by using C1s of graphite at 284.6 eV as a reference. The first-principles plane-wave pseudopotential method implemented in the CASTEP package was employed to calculate the formation energy for Al-ion insertion.¹⁴ The formation energy is defined as:

$$E_f(Al) = E_{tot}[2Al + (MoO_3)(MoO_3)]/2 - E_{tot}[(MoO_3)(MoO_3)]/2 - 2 \cdot E_{tot}(Al)/2$$

Electrochemical measurement

The working electrodes (anode) were prepared by mixing active materials MoO₃ or PPy@MoO₃, acetylene black and polytetrafluoroethylene (PTFE) in a weight ratio of 8:1:1 with the help of ethanol. The mixture was pressed into a film, and then dried at 80 °C overnight under vacuum. After drying, the film was cut into many disks and then these disks were pressed onto a carbon rod to act as the working electrodes. The AC positive electrode was prepared by the same way as anode. The AC is obtained from Ningde Xinseng Chemical Industrial Ltd., Co., exhibiting a specific surface area of about 2800 m² g⁻¹ measured by BET method. The positive and negative electrodes were tested by cyclic voltammetry (CV) and galvanostatic charge-discharge tests in 0.5 mol l⁻¹ Al₂(SO₄)₃ in an aqueous medium using a conventional three-electrode cell, in which a carbon rod and a SCE was used as the counter and reference electrodes, respectively. From the charge and discharge curves, the specific capacitance (F g⁻¹) of electrode material was calculated using formula: $C = (I \cdot \Delta t) / (m \cdot \Delta U)$, where I is the current (A) used for charge/discharge cycling, Δt is the charge time (seconds), m is the mass (g) of active materials in the working electrode, ΔU is the operating potential window (V) during charge. In the Al-ion capacitor system, PPy@MoO₃ as anode and activated carbon (AC) as cathode were assembled in a two-electrode glass cell separated by non-woven cloth by using 0.5 mol l⁻¹ Al₂(SO₄)₃ solution as the electrolyte. The mass proportion of electrode materials used was optimized by the equivalence of charge stored in a single electrode measurement. Generally, the charge stored by each electrode can be determined by the equation of $q = C \cdot \Delta E \cdot m$, where C is the specific capacitance three-electrode cell test, ΔE is the potential range, m is the mass of the active material. These Al-ion capacitors were tested with the voltage window of 0-1.5 V using CV and galvanostatic charge-discharge techniques at different current densities, and the results were used to calculate the specific capacitance, energy density and power density of the device.

Results and discussion

Preparation method and Structure characterization

The preparation procedure of the virginal MoO₃ nanotubes and PPy coated MoO₃ (PPy@MoO₃) nanotubes is shown in Fig. 1. At first, the MoO_{3-x} was grown on carbon fibers (CFs) by a simple electrodeposition method. The nucleation and growth

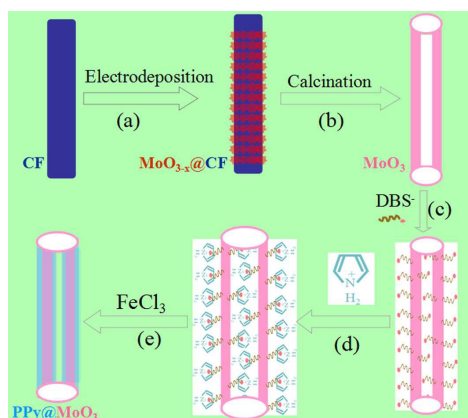


Fig. 1 Preparation process for the PPy@MoO₃ nanotubes.

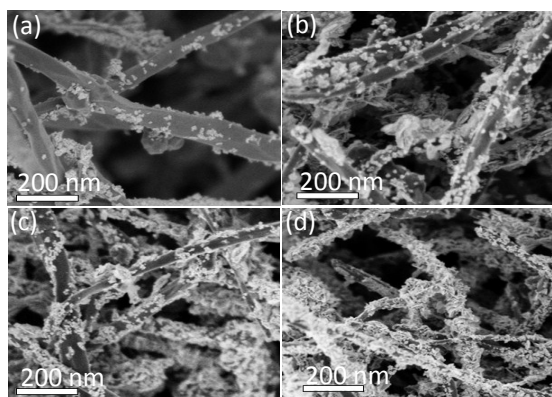


Fig. 2 SEM micrographs of the MoO_{3-x}@CF prepared from electrodeposition at different time (a) 1 min, (b) 2 min, (c) 3 min and (d) 5 min.

of MoO_{3-x} will preferentially take place on the surface of the CFs driven by minimizing the surface energy during the electrodeposition process. The scanning electron micrographs (SEM) of the samples (Fig. 2) after the electrodeposition show that more and more MoO_{3-x} nanoparticles were spontaneously assembled on the surface of the modified CFs with an increase in the electrodeposition times. Then the prepared MoO_{3-x}-coated CFs were further heat-treated at 500 °C for 5 hours. During the calcination process, the CFs were removed and the MoO_{3-x} nanoparticles were oxidized under air atmosphere and recrystallize to MoO₃ nanotubes. The PPy@MoO₃ nanotubes were prepared through the oxidation polymerization of pyrrole (Py) on the surface of the MoO₃ nanotubes using sodium dodecylbenzenesulfonate (NaDBS) as the surfactant and FeCl₃ as the oxidant.

The X-ray diffraction pattern of MoO₃ nanotubes (Fig. 3a) shows an orthorhombic structure (CPDS card No. 65-2421).²⁰ MoO₃ usually has orthorhombic, monoclinic, and hexagonal phases at room temperature. The orthorhombic structure is the only one that is thermodynamically stable. Moreover, it has a distinctive layer structure, and each layer is composed of [MoO₆]⁶⁻ octahedra in which each Mo atom is surrounded by a distorted oxygen octahedron. Interaction between adjacent layers is the weak van der Waals force. The strong intensities

of (0k0) family planes, i.e. (020), (040) and (060), relative to that of (021) plane indicate that the products have a preferred growth orientation in the b-axis.²⁰ The positions of the peaks of the PPy@MoO₃ nanotubes are consistent with those of the MoO₃ with no shift, indicating that there is no intercalation of PPy into layers of MoO₃. The TG curve (Fig. S1) shows a step decomposition of the PPy@MoO₃ nanotubes. The weight loss at 200 °C is due to the decomposition of the polymer component. When PPy was totally decomposed, a mass decrease rate of 9.7 wt.%, which corresponds to the amount of PPy coating, was detected.

SEM micrographs of the virginal MoO₃ and the PPy@MoO₃ are shown in Fig. 3b and c. As viewed from arrows, some tubular structure of these individual MoO₃ can be clearly observed. Moreover, some broken tubular crystals (insets in Fig. 3 b and c) further reveal the interior hollow space of these products. The tubular nanostructure of the sample was further convinced by transmission electron microscopy (TEM). The inner diameter of the nanotubes is about 40 nm, which is slightly smaller than that of the template (CFs). This suggests that the tubes slightly shrink during the high-temperature calcination process. Thickness of the PPy coating on the surface of MoO₃ nanotubes is about 10-15 nm (Fig. 3d), and the spacing between the adjacent lattice planes stacked along the growth direction is ca. 0.38 nm (Fig. 3e), which

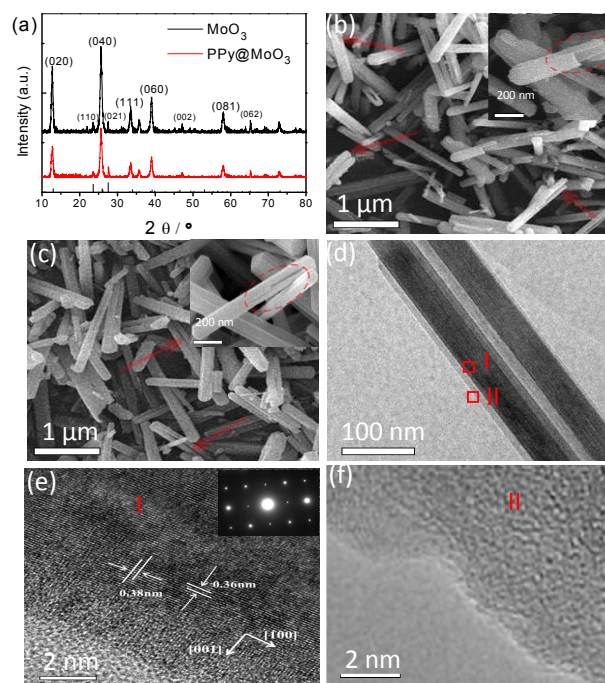


Fig. 3 Some physical properties of the virginal MoO₃ nanotubes and PPy@MoO₃ nanocomposite. (a) X-ray diffraction (XRD) pattern. SEM micrographs of the (b) MoO₃ nanotubes and (c) PPy@MoO₃ nanocomposite, (d) TEM, (e) and (f) HRTEM (high resolution TEM) micrographs of the PPy@MoO₃ nanocomposite.

corresponds to the distance of two (100) crystal planes (d_{100}).²⁰ The ED (electron diffraction) pattern of the corresponding MoO_3 in the inset of Fig. 3e demonstrates that the synthesized MoO_3 nanotubes are of highly crystalline. Different from MoO_3 , no crystalline morphology is detected in the HRTEM micrograph for PPy (Fig. 3f). In the ED pattern corresponding to PPy (Fig. S2), a broad and diffused halo ring was observed, which also indicates its amorphous phase.

Electrochemical properties of MoO_3 , PPy@ MoO_3 nanotubes

Some electrochemical performance of the prepared MoO_3 and PPy@ MoO_3 nanotubes is shown in Fig. 4. In the cyclic voltammetric (CV) curves of the MoO_3 nanotubes in $0.5 \text{ mol l}^{-1} \text{ Al}_2(\text{SO}_4)_3$ electrolyte (Fig. 4a), there are some pairs of redox peaks which is similar to pseudocapacitive characteristic. In case of the CV curve of AC (Fig. S3a), it exhibits the typical rectangular shapes as expected, indicating of electric double layer capacitance. The redox behavior of PPy in $\text{Al}_2(\text{SO}_4)_3$ electrolyte is weak in this potential range. As to the CV curve for the PPy@ MoO_3 nanotubes, its shape is similar to that of the MoO_3 nanotubes. When the scan rate increases from 1 to 5 mV s^{-1} , the anodic and cathodic peaks shift to higher and lower potentials, respectively. However, compared to the disappeared redox peaks for the MoO_3 nanotubes when the scan rate is increased to 5 mV s^{-1} (Fig. S3b), the redox peak potential for the PPy@ MoO_3 nanotubes shifts only 98 mV. This is because of the low polarization arising from the excellent electronic conductivity of the PPy coating. Two distinct discharging platforms at -0.2 and -0.3 V (vs. SCE) (Fig. 4b) can be found at 1 A g^{-1} , which is consistent with the CV curves. As

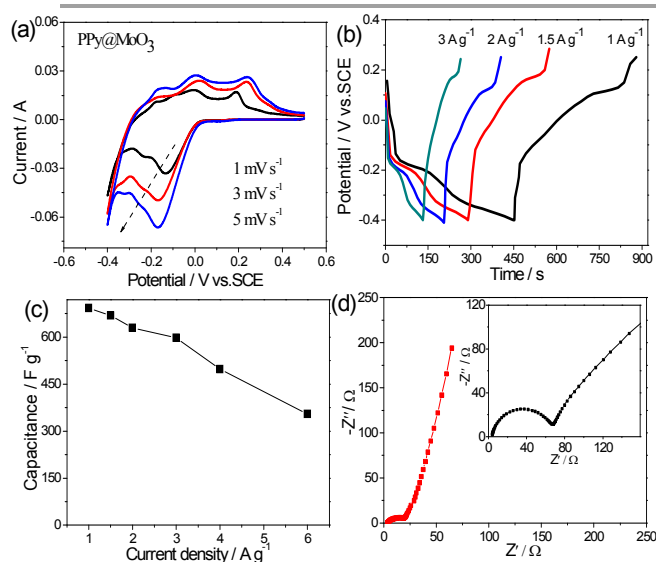


Fig. 4 Electrochemical properties of the prepared MoO_3 nanotubes and PPy@ MoO_3 nanocomposite. (a) CV curves of the MoO_3 @PPy nanotubes in $0.5 \text{ mol l}^{-1} \text{ Al}_2(\text{SO}_4)_3$ electrolyte at different scan rate, (b) galvanostatic charge/discharge curves (c) specific capacitance of the PPy@ MoO_3 nanotubes at different current densities, and (d) Nyquist plots of the PPy@ MoO_3 nanocomposite and the MoO_3 nanotubes (inset).

shown in Fig. 4c, the specific capacitances of the PPy@ MoO_3 nanotubes are 693, 669, 630, and 598 F g^{-1} , respectively, at current densities of 1, 1.5, 2, and 3 A g^{-1} , which are higher than those of the pure MoO_3 nanotubes electrode at the corresponding current density (Fig. S4). This is because that the PPy in the composites can provide high electronic conductivity of the overall electrode, which can also be proved by the electrochemical impedance spectroscopy (EIS) studies of the MoO_3 and the PPy@ MoO_3 nanotubes in Fig. 4d. Both show similar EIS profiles, with a semicircle in the high-frequency region and a straight line in the low-frequency region. The charge-transfer resistance (R_{ct}) is estimated to be 20 Ohm for the PPy@ MoO_3 electrode, which is noticeably lower than that for the MoO_3 electrode (65 Ohm).

Explanation of the electrochemical performance

When the electrolyte is replaced with $1.5 \text{ mol l}^{-1} \text{ Na}_2\text{SO}_4$ or $0.005 \text{ mol l}^{-1} \text{ H}_2\text{SO}_4$ electrolyte (near to the pH of 0.5 mol l^{-1}

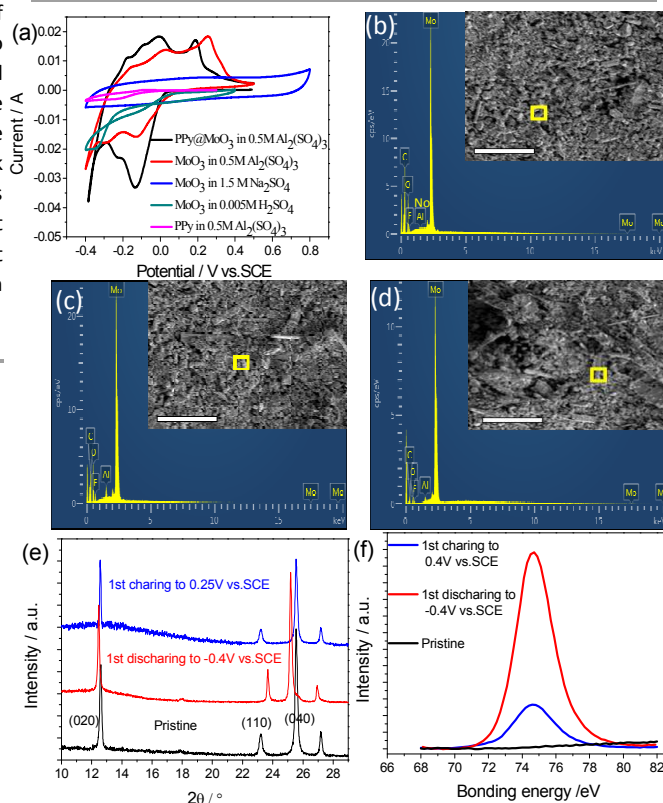


Fig. 5 (a) CV curves of the MoO_3 and the PPy@ MoO_3 nanotubes in different electrolytes at 1 mV s^{-1} . Energy dispersive X-ray spectroscopy (EDX) analyses of (b) pristine MoO_3 (before charging/discharging), (c) MoO_3 after 1st discharging to -0.4 V vs. SCE and (d) MoO_3 after 1st charging to 0.25 V vs. SCE. (e) XRD patterns of pristine MoO_3 (before charging/discharging), MoO_3 after 1st discharging to -0.4 V vs. SCE and MoO_3 after 1st charging to 0.25 V vs. SCE. (f) XPS spectrum of Al2p core levels. In order to eliminate the interference of the electrolyte, the sample of pristine MoO_3 was immersed into the electrolyte for 24h. Then it was washed with water.

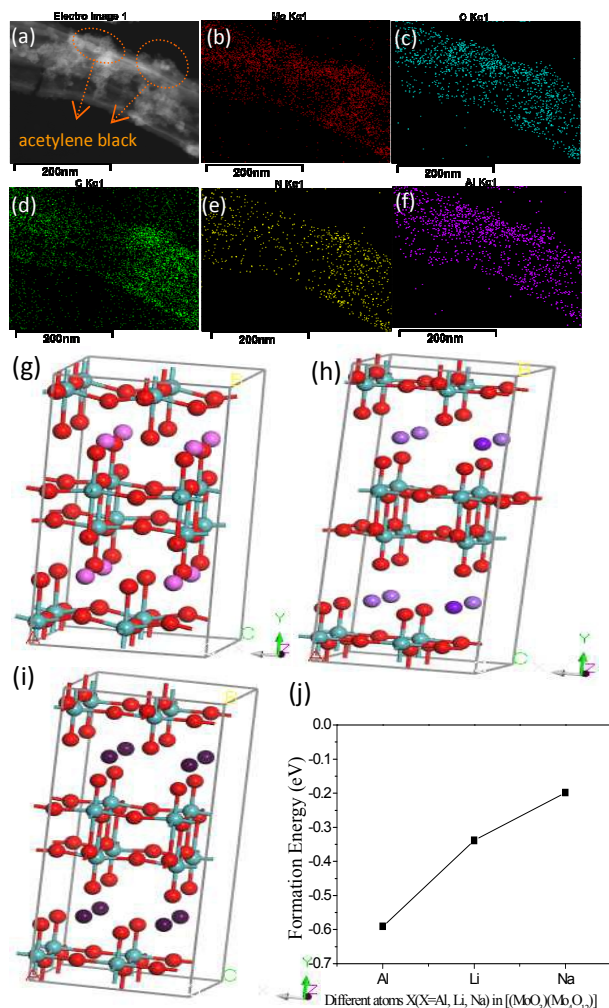


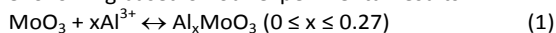
Fig. 6 (a) TEM micrographs of the electrode based on PPY@MoO₃ after discharging to -0.4 V vs. SCE, and the related elemental mappings: (b) Mo, (c) O, (d) C, (e) N and (f) Al. The atomic structures with different atoms in [(MoO₃)(Mo₄O₁₂)]: (g) Al, (h) Na, (i) Li. The red and blue balls correspond to Mo and O atoms, respectively. (j) The relationship between the formation energy and the different atoms in [(MoO₃)(Mo₄O₁₂)].

Al₂(SO₄)₃ electrolyte, about 2.0), the CV curves of the MoO₃ nanotubes exhibit an approximately rectangular and irregular shape, respectively, without any obvious redox peaks, and the area is very small (Fig. 5a). These results suggest that the redox peaks in 0.5 mol l⁻¹ Al₂(SO₄)₃ electrolyte are resulted from the Al³⁺ ions (or hydrated Al³⁺ ions) instead from SO₄²⁻ or H⁺ ions. Current change with the sweep rate can be generally expressed as: $i = av^b$, where i is the current (A) and v is the sweep rate (mV s⁻¹) of a cyclic voltammetric experiment, a and b are adjustable values.²¹ Fig. S5 presents a plot of log(i) versus log(v) for anodic peaks. For sweep rates ranging from 0.5 to 5 mV s⁻¹, the b -value for anodic peaks is about 1/2, indicating that the kinetic of MoO₃ in Al₂(SO₄)₃ electrolyte is a solid-state diffusion not just a surface-controlled diffusion.²¹

Although charge storage limited by solid-state diffusion is more common in intercalation compounds for Li ion battery in organic electrolyte and their rate capability is usually not good, here we use aqueous electrolyte together with the nanotubes structure and the its rate capability may be improved. Very recently, fast and highly reversible Al-ion intercalation in a prussian blue analog nanoparticles was achieved up to 300C in aqueous electrolyte.¹⁵ In this case, the redox peaks may be attributed to a multiple-stage Al³⁺ ions extraction/insertion from/into the layered MoO₃. Two-phase reaction mechanism for chemical insertion of Li⁺ and Mg²⁺ into α -MoO₃ was previously reported.^{22,23} The state of the MoO₃ nanotubes during the charging/discharging process is analyzed by EDX spectra, ex situ XRD and XPS spectra. The SEM micrographs and relevant EDX spectra (Fig. 5 b-d) show the morphological effect of the electrochemical process on the MoO₃ electrodes. Primary MoO₃ nanotubes of about 100 nm are uniformly dispersed with the acetylene black and PVDF. After the first discharging to -0.4 V (vs. SCE), only minor morphological changes were observed. The presence of Al is clearly identified by the EDX spectrum (Fig. 5c). After one full discharge/charge cycle, the morphology of the electrode resembles that of the pristine one and only a small amount of Al can be detected by EDX spectrum (Fig. 5d). However, due to the limit of this technique it is impossible to distinguish between surface and bulk origin of the Al peaks. Then the structural changes in the MoO₃ during the charging and discharging were monitored with XRD (Fig. 5e). After discharging to -0.4 V (vs. SCE), the main (020) peak of MoO₃ was shifted by 0.1–0.2° to lower angle and broadened. The shift of the (020) peak to lower angle can be directly associated with the increased in the interlayer distance, because the interlayers of MoO₃ are stacked along the <010> direction. Upon one full discharge/charge cycle, the peaks are nearly restored to the original positions. This peak shift is similar to the report on Mg²⁺ ion intercalation along the (020) layers of the MoO₃ electrodes.²³ The finding also indicates that the Mg_xMoO₃ phase is preferably developed on the surface of the MoO₃ particles while a portion of unreacted MoO₃ phase remains in the core of the particles.²³ But different from the Mg²⁺ ion intercalation into MoO₃, no distinct new peaks are found after discharging to -0.4V (vs. SCE). This may suggest that the charge/discharge process during Al³⁺ ions insertion and extraction may involve solid-solution reaction mechanism. From the XPS spectra of the surface state of the MoO₃ after the Al ion insertion (Fig. 5f), it can be seen that after the 1st discharging to -0.4 V (vs. SCE), the Al³⁺ (Al2p peak: 74.3 eV) appear. After one full discharge/charge cycle, there is a little of Al(III) on the surface of the MoO₃. This result is consistent with the EDX spectra in Fig. 5, which mean not all the Al ions inserted into the α -MoO₃ can be extracted and the coulombic efficiency during the first cycle is not 100%, only about 98%.

The Al³⁺ ions insertion is also confirmed by elemental mapping (Fig. 6a-f). The Al concentration is uniformly distributed within particles in the scanned area and matches well with the Mo and O distributions. To investigate the various electrochemical activities of the MoO₃ in Na₂SO₄ and

$\text{Al}_2(\text{SO}_4)_3$ electrolyte (Fig. 5a), we conducted density function theory calculations on their interaction with the Mo and O atoms (Fig. 6 g-i). MoO_3 has an orthorhombic structure with Pbnm symmetry group, composing of $[\text{MoO}_6]^{6-}$ octahedral units. The formation energy calculated by first-principles simulations with respect to the Al, Na, Li ions in MoO_3 is shown in Fig. 6j. Al ions show the most negative formation energy, indicating that the intercalation of Al^{3+} ions into MoO_3 can take place more easily in theory. This reaction is described as the following based on our experimental results:



Electrochemical properties of the assembled Al-ion capacitor

The charging/discharging curves of the two-electrode cell by using activated carbon (AC) as the cathode at 30 mA g^{-1} (Fig. S6) indicate that their combination as Al-ion capacitors is able to afford devices with an operation voltage of 1.5 V. The cut-off potentials for MoO_3 and AC were set at -0.4 and 1.1 V (vs. SCE), respectively. This can achieve a capacity of about 155 mAh g^{-1} for the MoO_3 anode and 48 mAh g^{-1} for the AC cathode. The balancing mass ratio of the anode to the cathode was designed to be 3.1 : 1 based on their capacities. Fig. 7 shows the electrochemical performance of the Al-ion capacitor based on the PPy@MoO_3 nanotube as the anode and AC as the cathode in aqueous $\text{Al}_2(\text{SO}_4)_3$ electrolyte. Prior to the assembly of the Al-ion capacitor, the anode (MoO_3 and PPy@MoO_3) was preconditioned in half-cells. They were firstly galvanostatically (1 A g^{-1}) cycled twice between $-0.4 - 0.25 \text{ V}$ (vs. SCE), and then discharged to a cut-off voltage of -0.4 V (vs. SCE). From the CV curves of the Al-ion capacitor based on the PPy@MoO_3 nanotubes and AC at various scan rates ranging

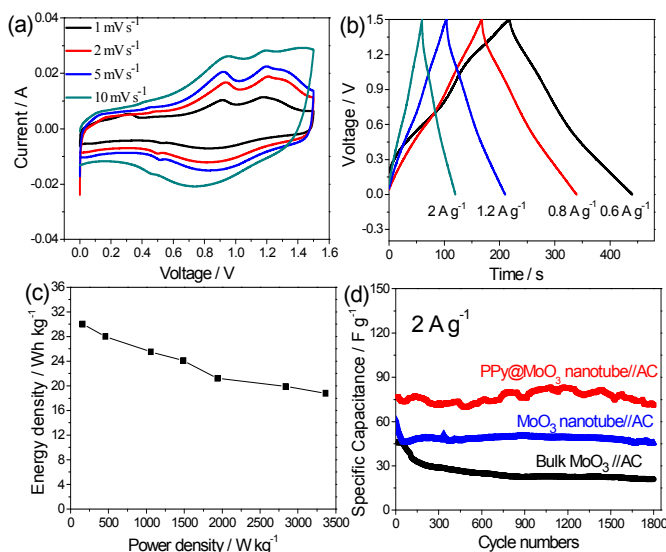


Fig. 7 Electrochemical performance of the assembled Al-ion capacitor. (a) CV curves, (b) galvanostatic charge/discharge curves from 0 to 1.5 V at different current densities, (c) Ragone plots, and (d) the cycling behavior at the current density of 2 A g^{-1} . The energy and power densities and capacitance were calculated based on the total weights of the cathode and anode materials.

from 1 to 10 mV s^{-1} measured between 0 and 1.5 V (Fig. 7a), some broad redox peaks are observed indicating the faradaic pseudocapacitive nature of the $\text{PPy@MoO}_3//\text{AC}$ capacitor arising from the MoO_3 electrode. Even at a scan rate of 10 mV s^{-1} , the CV curve still has obvious redox peaks during the charge or discharge process, suggesting the superior high-rate capability of the prepared Al-ion capacitor.

The Al-ion capacitor delivers no obvious voltage drop from its internal resistance (Fig. 7b), indicating the internal resistance for the Al-ion capacitor is very low. Remarkably, up to 73% of the capacitance can still be retained even the discharge current density is increased for 6 times (Fig. S7). As Fig. 7c shown, its energy density is up to 28 Wh kg^{-1} at a power density of 460 W kg^{-1} . It can still be 20 Wh kg^{-1} even at 2840 W kg^{-1} . Apparently, the energy density of this Al-ion capacitor is higher than those of recently reported asymmetric supercapacitors in aqueous electrolytes.²⁴ About 93% capacitance can still be retained even after 1800 cycles for the Al-ion capacitor ($\text{PPy@MoO}_3//\text{AC}$) (Fig. 7d). The coulombic efficiency of this Al-ion capacitor reaches almost 100% after the initial cycles (Fig. S8).

The exploration of Al ion insertion/extraction reactions may provide alternatives to current Li and Na ion based system for energy conversion and storage in the future. Very recently, it was reported that Ti_3C_2 showed spontaneous intercalation of cations (H^+ , Na^+ , K^+ , NH_4^+ , Mg^{2+} and Al^{3+}) from aqueous salt solutions.^{17,25,26} These work open up exciting possibilities of developing intercalation electrode materials for metal-ion capacitors. However, the Ti_3C_2 only delivers a low capacitance in aqueous $\text{Al}_2(\text{SO}_4)_3$ electrolyte.¹⁷ Prussian blue analogues (PBA) are another electrode materials for Al ion insertion in aqueous electrolyte.^{15,27} Unfortunately, its specific capacity is still low ($<60 \text{ mAh g}^{-1}$) which is only close to 0.2 Al^{3+} intercalation/deintercalation per formula unit of PBA. Vanadium oxides may be a kind of potential electrode material for Al ion insertion in aqueous electrolyte because of its high specific capacity in ionic liquid electrolyte.^{13,14} However, the toxicity of vanadium oxides makes these compounds useless in future application. In case of the single electrode (Fig. 4c) in this work, the maximum specific capacitance of the PPy@MoO_3 nanotubes for Al^{3+} ions is 693 F g^{-1} . This is much higher than those of recently reported carbon nanotubes@ MoO_3 nanosheets for Li^+ ions (500 F g^{-1})²⁸ and MoO_3 nanorods for Na^+ ions (214 F g^{-1}).²⁹ The main reason is due to: (1) the smaller diameter of Al^{3+} ions (53.5 pm) than those of Li^+ ions (76 pm) and Na^+ ions (102 pm) and (2) larger charge number per metal unit. Moreover, $\alpha\text{-MoO}_3$ is one of the most important layered materials and n-type metal oxide semiconductors. The shape, size, and crystal structure of MoO_3 can significantly influence the performance of electrochemical energy devices.^{30,31} In our previous work, LiMn_2O_4 nanotube with a preferred orientation of (400) planes shows excellent rate capability with 54% capacity after only 6 seconds for charging time.³² Here, by combining the electrodeposition with CFs template, the MoO_3 nanotubes with preferred orientation were also prepared successfully, which is different from the reported branchlike MoO_3/PPy ³³ and PPy coated MoO_3

nanobelts^{34a} and nanoplates^{19a} as electrode materials for conventional supercapacitor. Among various morphologies, one-dimensional (1D) nanotubes are of great interest due to its unique structural features. Besides 1D electron transport pathways, the hollow channels can buffer mechanical strain that would be generated during the cycling process.^{34b} Moreover, the interior tubular structures can provide more active sites for the electrolyte ions to achieve closer contact with the active material, thus increasing the utilization of the active material.³⁴

The excellent cycling behavior of the as-prepared PPy@MoO₃ nanotubes could be attributed to the PPy coating layer and 1D MoO₃ nanotubes structure. The cycling behavior of the Al-ion capacitor (about 93% of the initial capacity after 1800 cycles) is competitive to those of the latest reported Na-ion capacitors, such as Na₂Fe₂(SO₄)₃/Ti₂CT_x (about 83% of the initial capacity after 100 cycles),²⁵ AC//V₂O₅-CNT (80% of the initial capacity after 900 cycles),³⁵ and AC//Na₂Ti₃O₇ nanotube (80% of the initial capacity after 1000 cycles).³⁶ The MoO₃ nanotubes display a moderate cycling life with 25% fading of its initial specific capacitance after 1800 cycles (Fig. 6d), which is much better than MoO₃ nanobelt and nanoplates.^{18c,34a} The advantage of nano tubular MoO₃ electrode material, which can buffer the volume change during the charge and discharge process, is verified. In addition, the coated PPy can absorb the small amount of acid from the hydrolysis of 0.5 mol l⁻¹ Al₂(SO₄)₃ electrolyte, which is partially evidenced from the decrease of the charge transfer resistance of the PPy@MoO₃ electrode (Fig. 4d), and avoid acid etching of MoO₃. In the case of the bulk MoO₃, the specific capacitance sharply decreases after the initial 150 cycles and only ca. 40% of its initial capacitance is retained after 1800 cycles. This can be ascribed to two reasons: (1) the large volume expansion and shrinkage during the repeated charge-discharge process; and (2) the acid etching for the MoO₃ bulk.³⁷

Two fabricated (-)PPy@MoO₃//AC(+) Al-ion capacitors were connected as an energy storage unit. After being fully charged, the unit can drive two red LED segment display (Fig. 8). It should be noted that it is possible to further increase the

energy density of the Al-ion capacitor by optimizing the design of the cathode. In this work, the AC-based cathode exhibits low specific capacitance. Currently, most of the potential candidates with reversible electrochemical intercalation/deintercalation of Al³⁺ ions are below 0 V (vs. SCE).^{13-17,38} Thus, the development of cathode materials with high specific capacitance for Al-ion capacitor is a vital topic in the future.¹⁶ In addition, recently we reported a Na-ion capacitor assembled by a capacitor-type electrode and a Na-ion intercalation electrode.³⁹ Moreover, excellent sodium storage in α-MoO₃ anode material was demonstrated by others.^{40,41} Therefore, we believe that our α-MoO₃ nanotubes also show great potential application in Na-ion capacitors in the future.

Conclusions

In summary, we report an Al-ion capacitor, which is enabled by MoO₃ nanotubes coated by PPy (PPy@MoO₃) as the anode together with an activated carbon (AC) cathode in Al₂(SO₄)₃ aqueous solution. The PPy@MoO₃ presents a remarkable high capacitance of 693 F g⁻¹ for Al³⁺ ions, much higher than those of MoO₃ for Li⁺ and Na⁺ ions. This Al-ion capacitor achieves an energy density of 30 Wh kg⁻¹ based on the total mass of cathode and anode materials. The excellent cycling stability with 93% retention of the initial specific capacitance after 1800 cycles is competitive to those of the latest reported Li-/Na-ion capacitors. The main reason is ascribed to the unique PPy-coated nanotube structure. As an energy storage unit it could drive LEDs. The proposed Al-ion capacitor is expected to be a highly promising candidate for energy storage systems due to the most abundant resource of Al among all the metal elements.

Acknowledgements

Financial support from National Distinguished Young Scientists Program of NSFC (51425301) is gratefully appreciated.

Notes and references

- (a) D. Larcher and J. M. Tarascon, *Nat. Chem.*, 2015, **7**, 19–29; (b) F. Wang, S. Xiao, M. Li, X. Wang, Y. Zhu, Y. Wu, A. Shirakawa and J. Peng, *J. Power Sources*, 2015, **287**, 416–421; (c) X. Y. Xiao, Y. Q. Yang, M. X. Li, F. X. Wang, Z. Chang, Y. P. Wu and X. Liu, *J. Power Sources*, 2014, **270**, 53–58; (d) Y. S. Zhu, S. Y. Xiao, M. X. Li, Z. Chang, F. X. Wang, J. Gao and Y. P. Wu, *J. Power Sources*, 2015, **288**, 368–375.
- (a) B. E. Conway, *Electrochemical Supercapacitors-Scientific Fundamentals and Technological Applications* (Kluwer Academic/Plenum Publishers, 1999); (b) J. Wang, J. Huang, R. Yan, F. Wang, W. Cheng, Q. Guo and J. Wang, *J. Mater. Chem. A*, 2015, **3**, 3144–3150; (c) F. Yu, L. Zhu, T. You, F. Wang and Z. Wen, *RSC Adv.*, 2015, **5**, 96165–96169; (d) S. Xiao, F. Wang, Y. Yang, Z. Chang and Y. Wu, *RSC Adv.*, 2014, **4**, 76–81.
- S. Tasaki, N. Ando, M. Nagai, A. Shirakami, K. Matsui and Y. Hato, *Lithium ion capacitor*, WO 2006/112068 (2006).
- H. Tanizaki, N. Ando and Y. Hato, *Lithium-ion capacitor*, EP1914764A1 (2007).

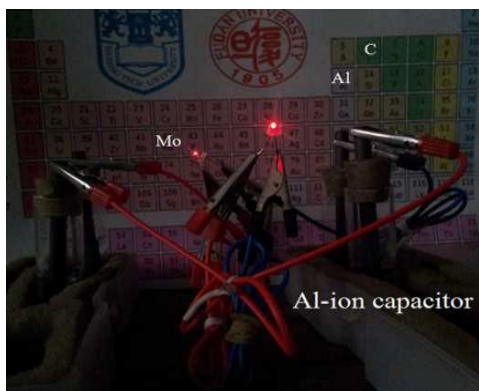


Fig. 8 An optical photograph showing two red LED were lighted, which were powered by this Al-ion capacitor.

- 5 (a) H. Wang, C. Guan, X. Wang and H. J. Fan, *Small*, 2015, **11**, 1470–1477 (b) C. M. Ghimbeu, C. Decaux, P. Brender, M. Dahbi, D. Lemordant, E. R. Pinerro, M. Anouti, F. Béguin and C. V. Guterl, *J. Electrochem. Soc.*, 2013, **160**, A1907–A1915.
- 6 (a) X. Yu, C. Zhan, R. Lv, Y. Bai, Y. Lin, Z. H. Huang, W. Shen, X. Qiu, F. Kang, *Nano Energy*, 2015, **15**, 43–53; (b) X. Wang, G. Shen, *Nano Energy*, 2015, **15**, 104–115; (c) K. Naoi, S. Ishimoto, J. Miyamoto and W. Naoi, *Energy Environ. Sci.*, 2012, **5**, 9363–9373.
- 7 (a) Y. Ma, H. Chang, M. Zhang, and Y. Chen, *Adv. Mater.* 2015, **27**, 5296–5308; (b) G. Gourdin, P. H. Smith, T. Jiang, T. N. Tran and D. Qu, *J. Electroanal. Chem.*, 2013, **688**, 103–112; (c) A. Jain, V. Aravindan, S. Jayaraman, P. S. Kumar, R. Balasubramanian, S. Ramakrishna, S. Madhavi, M. P. Srinivasan, *Sci. Rep.*, 2013, **3**, 3002–3007.
- 8 V. Aravindan, J. Gnanaraj, Y. S. Lee and S. Madhavi, *Chem. Rev.*, 2014, **114**, 11619–11635.
- 9 (a) H. Kim, J. Hong, K.Y. Park, H. Kim, S. W. Kim and K. Kang, *Chem. Rev.*, 2014, **114**, 11788–11827; (b) F. Wang, S. Xiao, Z. Chang, Y. Yang and Y. Wu, *Chem. Commun.*, 2013, **49**, 9209–9211; (c) F. X. Wang, S. Y. Xiao, Y. Shi, L. L. Liu, Y. S. Zhu, Y. P. Wu, J. Z. Wang, R. Holze, *Electrochim. Acta*, 2013, **93**, 301–306.
- 10 (a) Q. T. Qu, Y. Shi, S. Tian, Y. H. Chen, Y. P. Wu, R. Holze, *J. Power Sources*, 2009, **194**, 1222–1225; (b) J. L. Liu, L. L. Zhang, H. B. Wu, J. Y. Lin, Z. X. Shen and X. W. Lou, *Energy Environ. Sci.*, 2014, **7**, 3709–3719.
- 11 F. X. Wang, S. Y. Xiao, Y. S. Zhu, Z. Chang, C. L. Hu, Y. P. Wu and R. Holze, *J. Power Sources*, 2014, **246**, 19–23.
- 12 Q. Qu, P. Zhang, B. Wang, Y. Chen, S. Tian, Y. Wu and R. Holze, *J. Phys. Chem. C*, 2009, **113**, 14020–14027.
- 13 N. Jayaprakash, S. K. Das and L. A. Archer, *Chem. Commun.*, 2011, **47**, 12610–12612.
- 14 W. Wang, B. Jiang, W. Xiong, H. Sun, Z. Lin, L. Hu, J. Tu, J. Hou, H. Zhu and S. Jiao, *Sci. Rep.*, 2013, **3**, 3383–3388.
- 15 Z. Li, K. Xiang, W. Xing, W. C. Carter and Y. M. Chiang, *Adv. Energy Mater.*, 2015, **5**, 1401410–1401415.
- 16 (a) M. C. Lin, M. Gong, B. Lu, Y. Wu, D. Y. Wang, M. Guan, M. Angell, C. Chen, J. Yang, B. J. Hwang and H. Dai, *Nature*, 2015, **520**, 324–328; (b) S. Liu, J. J. Hu, N. F. Yan, G. L. Pan, G. R. Li and X. P. Gao, *Energy Environ. Sci.*, 2012, **5**, 9743–9746; (c) F. Wang, F. Yu, X. Wang, Z. Chang, L. Fu, Y. Zhu, Z. Wen, Y. Wu and W. Huang, *ACS Appl. Mater. Interfaces*, 2016, DOI: 10.1021/acsami.5b06142.
- 17 M. R. Lukatskaya, O. Mashtalir, C.E. Ren, Y. D. Agnese, P. Rozier, P. L. Taberna, M. Naguib, P. Simon, M. W. Barsoum, Y. Gogotsi, *Science*, 2013, **341**, 1502–1505.
- 18 (a) Y. N. Ko, S. B. Park, K. Y. Jung and Y. C. Kang, *Nano Lett.*, 2013, **13**, 5462–5466; (b) X. Peng, K. Huo, J. Fu, B. Gao, L. Wang, L. Hu, X. Zhang and P. K. Chu, *ChemElectroChem*, DOI : 10.1002/celc.201402349; (c) X. Xiao, T. Ding, L. Yuan, Y. Shen, Q. Zhong, X. Zhang, Y. Cao, B. Hu, T. Zhai, L. Gong, J. Chen, Y. Tong, J. Zhou and Z. L. Wang, *Adv. Energy Mater.*, 2012, **2**, 1328–1332; (d) X. Xiao, Z. Peng, C. Chen, C. Zhang, M. Beidaghi, Z. Yang, N. Wu, Y. Huang, L. Miao, Y. Gogotsi and J. Zhou, *Nano Energy*, 2014, **9**, 355–363; (e) F. Jiang, W. Li, R. Zou, Q. Liu, K. Xu, L. An and J. Hu, *Nano Energy*, 2014, **7**, 72–79; (f) Q. Mahmood, W. S. Kim and H. S. Park, *Nanoscale*, 2012, **4**, 7855–7860.
- 19 (a) W. Tang, L. L. Liu, Y. S. Zhu, H. Sun, Y. P. Wu and K. Zhu, *Energy Environ. Sci.*, 2012, **5**, 6909–6913; (b) D. Hanlon, C. Backes, T. M. Higgins, M. Hughes, A. O. Neill, P. King, N. McEvoy, G. S. Duesberg, B. M. Sanchez, H. Pettersson, V. Nicolosi and J. N. Coleman, *Chem. Mater.*, 2014, **26**, 1751–1763.
- 20 L. Cai, P. M. Rao and X. Zheng, *Nano Lett.*, 2011, **11**, 872–877.
- 21 (a) L. Z. Li, J. Ding, H. Wang, K. Cui, T. Stephenson, D. Karpuzov and D. Mitlin, *Nano Energy*, 2015, **15**, 369–378; (b) H. Kim, J. Hong, Y. U. Park, J. Kim, I. Hwang and K. Kang, *Adv. Funct. Mater.*, 2015, **25**, 534–541.
- 22 A. M. Hashem, M. H. Askar, M. Winter, J. H. Albering and J. O. Besenhard, *Ionics*, 2007, **13**, 3–8.
- 23 G. Gershinsky, H. D. Yoo, Y. Gofer and D. Aurbach, *Langmuir*, 2013, **29**, 10964–10972.
- 24 G. Yu, L. Hu, M. Vosgueritchian, H. Wang, X. Xie, J. R. McDonough, X. Cui, Y. Cui and Z. Bao, *Nano Lett.*, 2011, **11**, 2905–2911.
- 25 X. Wang, S. Kajiyama, H. Iinuma, E. Hosono, S. Oro, I. Moriguchi, M. Okubo, A. Yamada, *Nat. Commun.*, 2015, **6**, 6544–6549.
- 26 M. Ghidui, M. R. Lukatskaya, M. Q. Zhao, Y. Gogotsi and M. W. Barsoum, *Nature*, 2014, **516**, 78–81.
- 27 S. Liu, G. L. Pan, G. R. Li and X. P. Gao, *J. Mater. Chem. A*, 2015, **3**, 959–962.
- 28 D. Hanlon, C. Backes, T. M. Higgins, M. Hughes, A. O. Neill, P. King, N. McEvoy, G. S. Duesberg, B. M. Sanchez, H. Pettersson, V. Nicolosi and J. N. Coleman, *Chem. Mater.*, 2014, **26**, 1751–1763.
- 29 Z. Cui, W. Yuan and C. M. Li, *J. Mater. Chem. A*, 2013, **1**, 12926–12931.
- 30 T. Brezesinski, J. Wang, S. H. Tolber and B. Dunn, *Nat. Mater.*, 2010, **9**, 146–151.
- 31 P. Meduri, E. Clark, J. H. Kim, E. Dayalan, G. U. Sumanasekera and M. K. Sunkara, *Nano Lett.* 2012, **12**, 1784–1788.
- 32 W. Tang, Y. Y. Hou, F. X. Wang, L. L. Liu, Y. P. Wu and K. Zhu, *Nano Lett.*, 2013, **13**, 2036–2040.
- 33 X. Zhang, X. Zeng, M. Yang and Y. Qi, *ACS Appl. Mater. Interfaces*, 2014, **6**, 1125–1130.
- 34 (a) Y. Liu, B. H. Zhang, Y. Q. Yang, Z. Chang, Z. B. Wen and Y. P. Wu, *J. Mater. Chem. A*, 2013, **1**, 13582–13587; (b) C. Wang, F. Wang, Y. Zhao, Y. Li, Q. Yue, Y. Liu, Y. Liu, A. A. Elzathary, A. Al-Enizi, Y. Wu, Y. Deng, and D. Zhao, *Nano Res.*, 2016, DOI 10.1007/s12274-015-0976-7; (c) F. Wang, Z. Chang, X. Wang, Y. Wang, B. Chen, Y. Zhu and Y. Wu, *J. Mater. Chem. A*, 2015, **3**, 4840–4845; (d) C. L. Hu, H. H. Yi, F. X. Wang, S. Y. Xiao, Y. P. Wu, D. Wang and D. L. He, *J. Power Sources*, 2014, **255**, 355–359.
- 35 Z. Chen, V. Augustyn, X. Jia, Q. Xiao, B. Dunn and Y. Lu, *ACS Nano*, 2012, **6**, 4319–4327.
- 36 J. Yin, L. Qi and H. Wang, *ACS Appl. Mater. Interfaces*, 2012, **4**, 2762–2768.
- 37 (a) W. Tang, Y. Zhu, Y. Hou, L. Liu, Y. Wu, K. P. Loh, H. Zhang and K. Zhu, *Energy Environ. Sci.*, 2013, **6**, 2093–2104; (b) F. X. Wang, S. Y. Xiao, X. W. Gao, Y. S. Zhu, H. P. Zhang, Y. P. Wu and R. Holze, *J. Power Sources*, 2013, **242**, 560–565; (c) F. Wang, Y. Liu, X. Wang, Z. Chang, Y. Wu and R. Holze, *ChemElectroChem*, 2015, **2**, 1024–1030.
- 38 J. Muldoon, C. B. Bucur and T. Gregory, *Chem. Rev.*, 2014, **114**, 11683–11720.
- 39 F. X. Wang, X. W. Wang, Z. Chang, X. W. Wu, X. Liu, L. J. Fu, Y. S. Zhu, Y. P. Wu and W. Huang, *Adv. Mater.*, 2015, **27**, 6962–6968.
- 40 S. Hariharan, K. Saravanan and P. Balaya, *Electrochem. Commun.*, 2013, **31**, 5–9.
- 41 Y. Dong, X. Xu, S. Li, C. Han, K. Zhao, L. Zhang, C. Niu, Z. Huang and L. Mai, *Nano Energy*, 2015, **15**, 145.

Journal Name

ARTICLE

Table of content:

A conductive polymer coated MoO₃ anode enables an Al-ion capacitor with high performance

Faxing Wang, Zaichun Liu, Xiaowei Wang, Xinhai Yuan, Xiongwei Wu, Yusong Zhu, Lijun Fu, and Yuping Wu

The feasibility of assembling an Al-ion capacitor with good electrochemical performance is demonstrated. Preliminary results indicate that the fabricated Al-ion capacitor could reversibly cycle in the voltage region of 0–1.5 V and displays intriguing performances. With an energy density of 30 Wh kg⁻¹. The proposed Al-ion capacitor is expected to be a highly promising candidate for energy storage systems due to the most abundant resource of Al among all the metal elements.

